Bull. Inst. Chem. Res., Kyoto Univ., Vol. 66, No. 3, 1988

Lattice Disorders in the Stereocomplex of Poly(L-lactide) and Poly(D-lactide)

Takumi OKIHARA*, Akiyoshi KAWAGUCHI*, Hideto TSUJI**, Soung-Hyu HYON**, Yoshito IKADA** and Ken-ichi KATAYAMA*

Received October 20, 1988

In the X-ray and electron diffraction patterns of drawn fibers of the stereocomplex of poly(L-lactide) and poly(D-lactide), the equatorial reflections were rather sharp, but those on the layer lines were largely broadened tailing in the direction parallel to the layer line, becoming more diffuse as the layer order increases. According to the paracrystalline theory, lattice disorders causing the broadening were analysed. The degree of shift disorder among polymer chains in the direction parallel to their molecular axis is estimated at about 0.1.

KEY WORDS: Stereocomplex/ Poly(L-lactide)/ Poly(D-lactide)/ Paracrystalline/ Lattice disorder/

INTRODUCTION

The equimolar mixture of poly(L-lactide) (PLLA) and poly(D-lactide) (PDLA) is crystallized into a stereocomplex with the unit cell of cell dimensions: a=0.916 nm, b=0.916 nm, c=0.870 nm, $\alpha=109.2°$, $\beta=109.2°$ and $\gamma=109.8°$, in which respective polymer chains in the 3_1 helical conformation are packed side-by-side in a pair in the parallel fashion [1]. The X-ray and electron diffraction patterns of the complex fiber are found to have the following characteristics; (1) the equatorial reflections are rather sharp up to the high order ones, and (2) the reflections on the layer lines are broadened tailing in the direction parallel to the layer line, being more diffuse with the increase of layer order. Most of drawn polymer fibers exhibit more or less these diffraction features; for example, in case of polyethylene, reflections on the second layer line are rather sharp up to higher reflection angle, where as in the fiber pattern of poly-β-propiolactone, reflections even on the first layer line degenerate into a diffuse streak [2]. The broadening behavior of diffractions on the layer lines is qualitatively explained in terms of the shift disorders among chains in the direction parallel to their molecular axis. In the present paper, the lattice disorders are semiquantitatively discussed on the basis of the paracrystalline theory [3,4], and broadening of diffractions on the layer lines is simulated by a computer.

* 沖原 巧, 河口昭義, 片山健一 : The Institute for Chemical Research, Kyoto University, Uji, Kyoto 611, Japan

** 辻 秀人, 玄 丞烋, 筏 義人 : Research Center for Medical Polymers and Biomaterials, Kyoto University, Kawaracho, Shogoin, Sakyo, Kyoto 606, Japan

EXPERIMENTAL

Thin films for electron microscopy were prepared by means of the Petermann and Gohil method [5] using the dilute solution in p-xylene, in which PLLA and PDLA were dissolved in a ratio of 1:1. Being less crystalline, as-prepared films were annealed at 198°C in N_2-atomosphere for 2 hrs to promote crystallization. Oriented specimens for X-ray diffraction works were made by drawing a cast film of PLLA and PDLA with their content ratio of 1:1. The drawn films were also annealed to grow the complex crystals further. Lamellar crystals of the complex were grown from the 0.1 wt% solution in acetonitrile in which PLLA and PDLA were disolved in the equimolar ratio[6].

Electron microscopic observations were carried out with an electron microscope JEM-200CS, JEOL, and X-ray diffraction work with a rotating anode X-ray generator RU-300, Rigaku. Cylindrical fiber photographs of the stereocomplex were taken using a filament 0.2 mm thick in diameter. To perform the profile analysis of the patterns, the integral breadth method was used. In order to correct the instrumental broadening, line profiles of the cylindrical photograph of an aluminium filament with the same diameter were utilized. The pure line breadths of the complex samples were obtained from the experimental breadths by subtraction of instrumental broadening on the assumption that as-measured line profiles of the polymer and aluminuim are expressed by the Lorentzian functions[7]. X-ray diffraction patterns were taken in a vacuum using CuK_α radiation monochromatized with a graphite crystal.

THEORETICAL BAIS

The scattering intensity of X-rays by matters is expressed in a general form [4];

$$I(\mathbf{s})=N(\langle Fu(\mathbf{s})^2\rangle-|\langle Fu(\mathbf{s})\rangle|^2\cdot D)+\frac{1}{v}|\langle Fu(\mathbf{s})\rangle|^2\cdot D\cdot Z(\mathbf{s})*|S(\mathbf{s})|^2 \qquad (1)$$

In the quation,

- $Fu(\mathbf{s})$: the scattering factor of a single scattering unit,
- v : the volume of the scattering unit,
- D : the factor due to the disorder of the first kind (Debye-Waller factor),
- $Z(\mathbf{s})$: the interference function (the lattice factor),
- $|S(\mathbf{s})|^2$: the shape factor,
- $\mathbf{s}$: the scattering vector ($|\mathbf{s}|=2\cdot\sin\theta/\lambda$ in which θ is the Bragg angle and λ the wavelength of X-ray),
- N : the number of scattering units in a coherent scattering volume,

and the symbols $\langle\ \rangle$ and $*$ mean the averaging and convolution operations, respectively. In the present case, the unit cell of the crystalline complex is taken as a scattering unit.

Lattice disorders or distorions of the second kind largely depend on the distribution of the centers of gravity of the scattering units(the unit cells) in a scattering matter. Their effect on the scattering intensity is involved in the interference function Z(s).

According to Hosemann's idea of paracrystalline structure, the entire distribution of scattering units in the whole matter can be expressed if the distribution functions of the nearest neighbours are known. On the basis of this theory, the lattice disorders of the second kind were examined. For convenience of further discussion, the Cartesian coordinates are set up with the z axis parallel to the direction of molecular axis as shown in Fig. 1, and the corresponding reciprocal space is described in X, Y and Z. The distributions of the nearest neighbours in the directions x, y and z in the real lattice coordinates are denoted by the functions $H_1(x, y, z)$, $H_2(x, y, z)$ and $H_3(x, y, z)$, respectively. (Thereafter, these functions are abbreviated to $H_i(i=1, 2, 3)$.) Lattice disorders in paracrystals are specified by the mean squares of fluctuations arround the averaged lattice points $\Delta_{ij}(i, j=1, 2, 3)$, where the first subscript denotes the function which the quantity is characteristic of and the second the coordinate axis along which the fluctuation occurs(1, 2 and 3 for x, y and z, respectively). The one-dimensional interference function $Z_i(X, Y, Z)(i=1, 2, 3)$ due to H_i in the corresponding direction in real space is defined and expressed in terms of the Fourier transform of the distribution function;

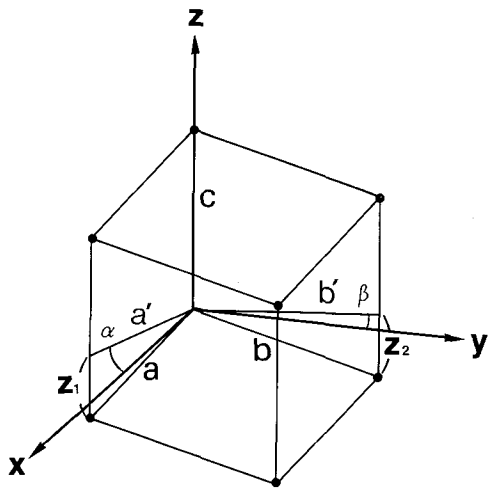

Figure 1. Parameters to specify the triclinic unit cell of PLLA and PDLA complex in the Cartesian coordinates. The origin is set at the center of gravity of a unit cell. The x and y axes are in the plane normal to the molecularaxis, and a′ and b′ are the projections of the **a** and **b** primitive translational vectors of the crystal lattice on the x-y plane. Small solid circles show the centers of gravity of neighboring unit cells. z_1 and z_2 are displacements of the neighboring centers in the a′ and b′ directions from the x-y plane, respectively. α and β are the angle between the a′ and x axes and that between b′ and y axes, respectively. In the present set-up of the coordinates, they are both 15°.

$$Z_i(\mathbf{s})=\mathrm{Re}\{(1+F_i(\mathbf{s}))/(1-F_i(\mathbf{s}))\} \tag{2}$$

where $F_i(\mathbf{s})$ denotes the Fourier transform of H_i, Re means the real part of the function and **s** stands for a vector **s**(X, Y, Z) in reciprocal space. In eq.(2), $F_i(\mathbf{s})$ is generally complex and represented with the moduli and phase; $F_i(\mathbf{s})=|F_i(\mathbf{s})|\exp(i\chi)$ and its

conjugated complex $F_i(\mathbf{s})^* = |F_i(\mathbf{s})| \exp(-i\chi)$, where $\chi = 2\pi\mathbf{s} \cdot \mathbf{a}_i$ in which $\mathbf{a}_i$ is the primitive translational vector in the i-axis of the crystal lattice. These are inserted in eq.(2) to give

$$Z_i(\mathbf{s}) = \frac{1 - |F_i(\mathbf{s})|^2}{1 - 2|F_i(\mathbf{s})| \cos\chi + |F_i(\mathbf{s})|^2} \tag{3}$$

The three dimensional interference function for an ideal paracrystal, where there is no correlation among the distribution functions in the respective axes, is expressed by the product of one-dimensional interference functions as $Z(\mathbf{s}) = Z_1(\mathbf{s})Z_2(\mathbf{s})Z_3(\mathbf{s})$.

In the eq. (1), the first term denotes the diffuse background intensity changing gradually with the scattering angle and the second term the crystalline reflections measured as the Bragg peaks. In order to estimate the lattice disorder and crystallite size, the profile analysis of the crystalline reflections is carried out. Though various methods have been put forward for this purpose, the integral method is adopted for its convenience [7]. The diffraction profile is mostly determined by the convolution of $Z(\mathbf{s}) * |S(\mathbf{s})|^2$ in eq. (1), for $F_u(\mathbf{s})$ and D dully affect the change in diffraction intensity with the change of the scattering angle. A peak profile of the function $Z(\mathbf{s})$ is well approximated by the Lorentzian function and that of the shape factor can be also replaced with the Lorentzian function. By this substitution of functions, the convolution can be easily performed and resultingly, the integral breadth $\delta\beta$ for a crystalline reflection is expressed by two terms attributed to the crystallite size and lattice disorder as follows[8]:

$$\delta\beta = \frac{1}{Nd} + \frac{(\pi gh)^2}{d} \tag{4}$$

where g is a disorder parameter defined as the ratio Δ/d of the lattice spacing d and its fluctuation Δ, N the number of the lattice planes and h the reflection order.

RESULTS AND DISCUSSION

Figures 2 and 3 show the electron and X-ray diffraction patterns of the drawn fiber of the complex of PLLA and PDLA, respectively. These fiber patterns show clearly

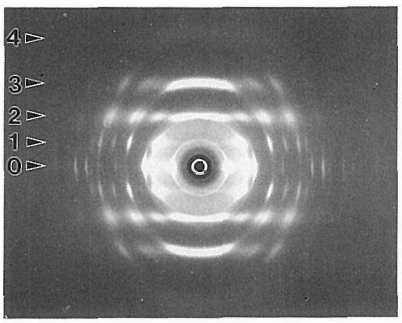

Figure 2. X-ray fiber pattern of the stereocomplex of PLLA and PDLA. The fiber axis is vertical. Figures on the left side show the order of layer line.

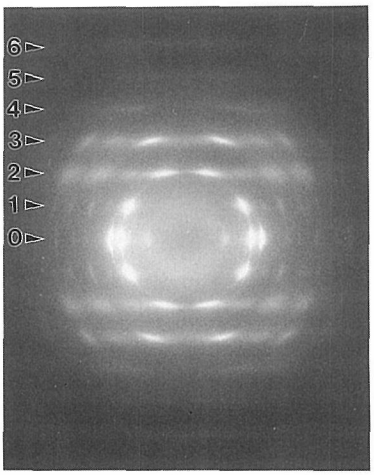

Figure 3. Electron diffraction pattern of the fiber of PLLA and PDLA. The fiber axis is vertical. Figures on the left side show the order of layer line.

the diffraction features outlined above in the introduction. Broadening and tailing of the reflections on the layer lines are more remarkable as the order of layer increases. Eventually, reflections on the layer line over the 4th one are so broadened to fuse with the background into a continuous diffuse streak. By applying the eq. (4) to the line broadening of equatorial reflections of the X-ray fiber pattern, the degree of paracrystalline lattice disorder and the crystallite size in the direction perpendicular to the molecular axis were first evaluated. Integral breadths of 100 to 500 reflections are plotted against the square of reflection order in Fig. 4. When the plot is linearly approximated by the eq. (4) against h^2, though data scatter in Fig. 4, the crystallite size

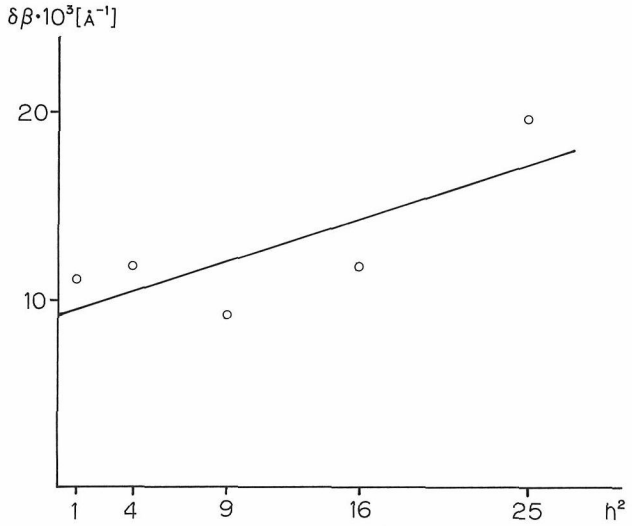

Figure 4. Integral breadths of *h*oo reflections as a function of the square of reflection order.

is estimated at 10.9 nm from its intercept with the ordinate and the g-value of disorder parameter 0.011 from the slope. As the hk0 net in reciprocal space is hexagonally symmetric (see below in Fig. 9), reflections indexed as 010 and $\bar{1}10$ overlap on the 100 reflections in the fiber pattern, and many reflections do so on the 200 to 500 reflections. As many reflections which are indexed with different Miller indices but have the same Bragg angle overlap into a single peak, the integral breadths are averaged and dispersed as seen in Fig. 4 so that some ambiguousness might be unavoidable in above results by the linear approximation. It is at least concluded, however, that the lateral order of molecular packing is very high because equatorial reflections remain sharp up to the high order. Since no meridional or near-meridional reflections with more than two different diffraction orders exist, the lattice disorder and crystallite size in the molecular direction, unfortunately, cannot be obtained in the above way. The shift disorder along the chain axis was estimated in the simulation procedure.

As analysed above using the equatorial reflections, the radial fluctuation in the x direction Δ_{11}, to which the value Δ_{22} in the y direction is probably equal, is 0.013 nm. Though the tangential components Δ_{12} and Δ_{21} cannot be obtained in the above way, they are considered to be nearly equal to Δ_{11} and Δ_{22}, as judged from the spotty electron diffractions without spreading in special directions (see Fig. 9). When values of these mean squares of fluctuations are all taken to be equal, fluctuations in the distances of nearest neighbouring molecules in x and y directions are radially symmetric, i.e. isotropic, around their axis. Normally, principal axes of the fluctuations are in the crystallographic axes. Though the present crystal has a triclinic system with the oblique lattice axes, the principle axes of fluctuations are taken to be in the x, y and z directions of the Cartesian coordinates. When the fluctuations are isotropic in the plane normal to the molecular axis as in the present case, the set-up of the orthogonal lattice coordinates will give rise to no serious error in description of fluctuations. The value of Δ_{33} is maybe small because the repeat distance of a polymer chain is constant in the fully extended conformation. It is assumed that Δ_{31} and Δ_{32} are very small. In view of the magnitude of these mean square of fluctuations, the distribution functions H_1, H_2 and H_3 can be expressed using the Gaussian functions in terms of the parameters in Fig. 1.

$$H_1(x, y, z)=\frac{1}{(2\pi)^{3/2}\Delta_{11}\Delta_{12}\Delta_{13}} \exp\left[-\frac{1}{2}\left\{\frac{(x-a'\cos\alpha)^2}{\Delta_{11}^2}+\frac{(y-b'\sin\alpha)^2}{\Delta_{12}^2}+\frac{(z-z_1)^2}{\Delta_{13}^2}\right\}\right]$$

$$H_2(x, y, z)=\frac{1}{(2\pi)^{3/2}\Delta_{21}\Delta_{22}\Delta_{23}} \exp\left[-\frac{1}{2}\left\{\frac{(x-b'\sin\beta)^2}{\Delta_{21}^2}+\frac{(y-b'\cos\beta)^2}{\Delta_{22}^2}+\frac{(z-z_2)^2}{\Delta_{23}^2}\right\}\right]$$

$$H_3(x, y, z)=\delta(x)\ \delta(y)\ \delta(z-c) \tag{7}$$

where δ means a delta function. The Fourier transforms of these functions can be easily obtained in the analytical form. The one-dimensional interference functions Z_1,

Z_2 and Z_3 are calculated by inserting the Fourier transforms of eqs. (5) to (7) in eq. (3), respectively. The three-dimensional interference function Z(s) is finally obtained by multiplying the three one-dimensional interference functions *when the present system is assumed to be an ideal paracrystal.* To ease the calculation, the crystallite size is assumed to be large enough to be approximated as $|(\mathbf{s})|^2 \rightarrow V \cdot \delta(\mathbf{s})$ where V is the volume of a crystllite. As estimated above, however, the lateral size of crystallites is finite in reality and surely produces broadening of reflections. The small, finite crystallites cause all reflections to broaden almost equally in the X and Y directions independently of the order of reflection or the reflection angle. Thus, profiles of the diffraction patterns were examined paying our attention to the dependence of line broadening on the order of reflection or the scattering angle. On the above assumptions, the intensity of the crystalline reflections in eq. (1) is simply expressed by

$$I(\mathbf{s}) = N|\langle Fu(\mathbf{s})\rangle|^2 \cdot D \cdot Z(\mathbf{s}) \tag{8}$$

In actual calculation, Fu(s) and D obtained by structure analysis were used, i.e., the isotropic temperature factor is 0.09 nm^2 [1]. To simulate the fiber pattern, the Cartesian coordinates (X, Y, Z) are transformed into the cylindrical ones (R, Ψ, Z) and the intensity function is averaged over the whole Ψ as follows;

$$I(R, Z) = \frac{1}{2\pi}\int_0^{2\pi} I(R, \Psi, Z)d\Psi \tag{9}$$

Following Hosemann [9], we assume that loss of crystalline reflections may be determined by the region in the diffraction pattern in which the intensity maxima do not exceed the back ground by more than 10–20%. When this criterion is applied to the disappearance of crystalline reflections on the layer line, the mean square of fluctuation by the shift disorder Δ_{ij} is estimated by the following relation in terms of the order of the boundary layer line, l, over which reflections are largely broadened to degenerate into a continuous broad streak; that is, $\Delta_{ij} = 0.25/l$ c where c is the primitive translation of the crystal c-axis. In consideration that reflections on the 4th order of layer line become a diffuse streak, g-value of the shift disorder in the PLLA and PDLA complex is evaluated at 0.062 by the relation, i.e. Δ_{13} and Δ_{23} are both 0.054 nm. Figure 5 shows the averaged line profiles of the fiber diffraction pattern, which are simulated by the eq. (9) using the the experimentally obtained or assumed values of mean squares of fluctuations. Peaks which can be identified as crystalline reflections still remain on the 4th layer line as seen in Fig. 5E. Even if broadening due to the small crystallites size (10.9 nm) is taken into account, the sharp peaks in Fig. 5E will not fuse into a diffuse streak. Figure 6 shows the two-dimensional intensity maps developed on the zeroth to fifth layer planes, which are simulated by the eq. (8). The intensity maxima are point-like on the zeroth layer plane and become expanding more and overlapping at their tails on the layer plane as the layer order increases. On the 4th layer plane, however, most of diffraction maxima still so sharp to be recognized as isolated peaks. Larger values of Δ_{13} and Δ_{23} for shift disorders are needed to make the simulated profiles closer to the really observed ones. Figure 7 shows the diffraction profiles simulated by using the g-value of 0.1, i.e. 0.087 nm for Δ_{13} and Δ_{23} (other Δ's are

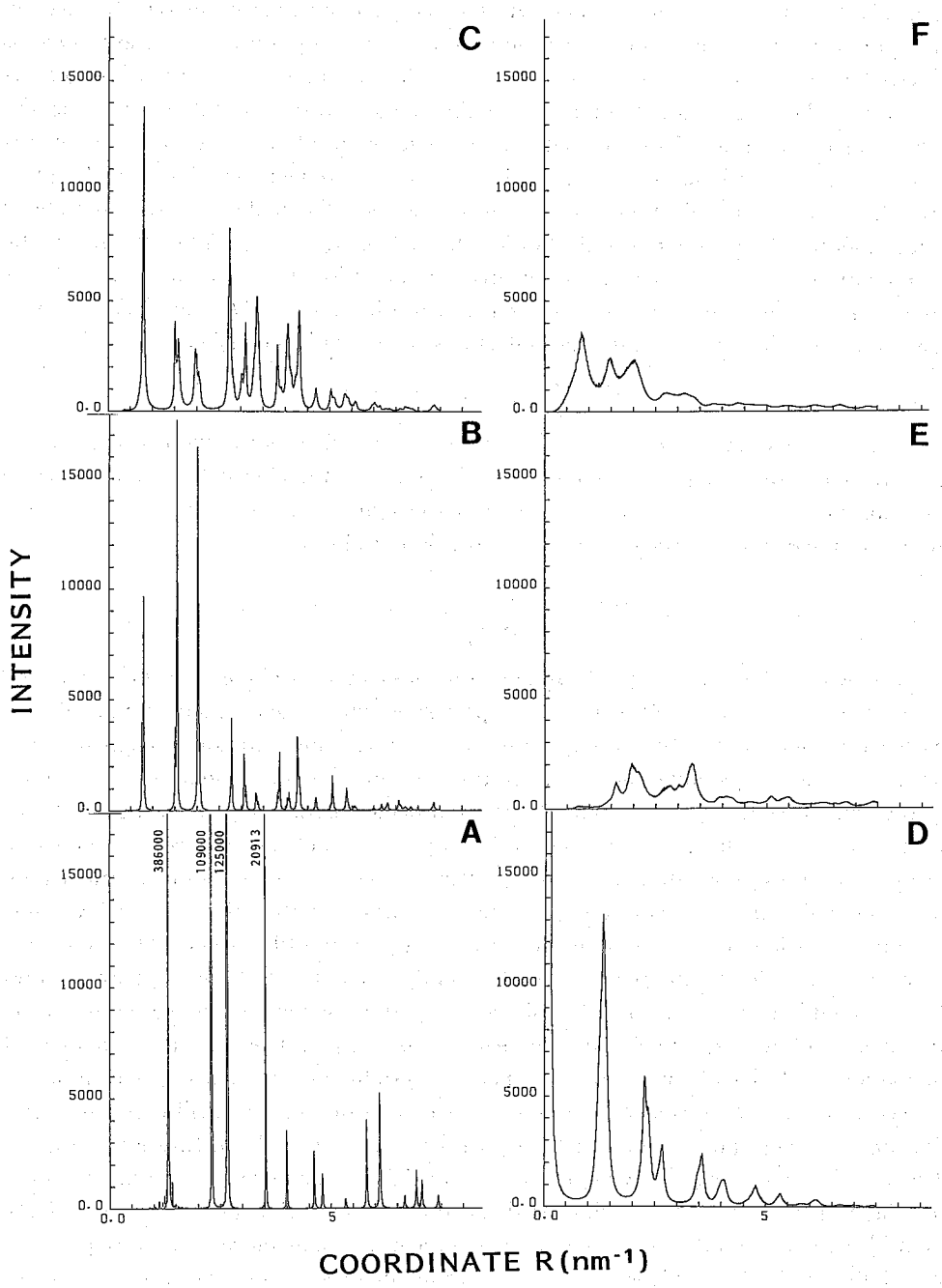

Figure 5. Patterns of A to F shows the calculated X-ray diffraction profiles on the zeroth to fifth layer lines, respectively.

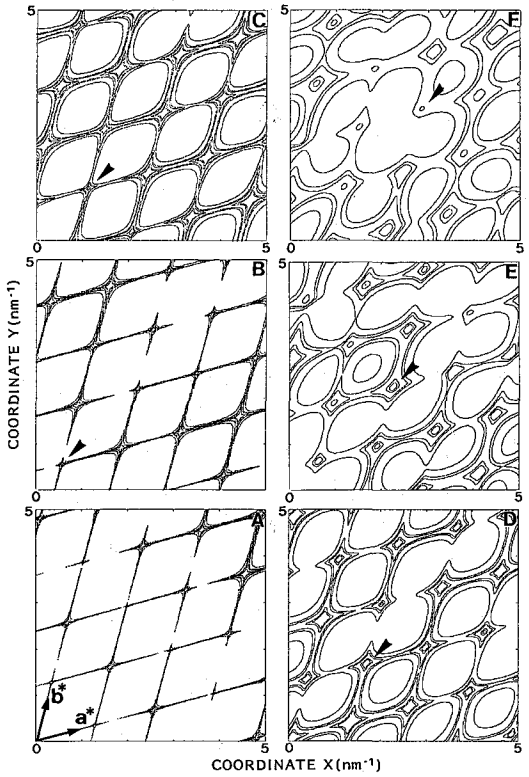

Figure 6. Simulated intensity maps developed on the layer planes. Maps of A to F correspond to the profiles of A to F in Fig. 5, respectively. Contour lines are drawn at the intensities of 100, 500, 1000, 5000 and 10000. The reciprocal axes a* and b* of the unit cell are shown by arrows in A. Positions shown by arrows in B to F correspond to 001, 002, 003, 004 and 005 reciprocal points, respectively.

unchanged), and Fig. 8 the corresponding contour maps of diffraction intensity on the layer planes. In Fig. 7 crystalline diffraction peaks are no longer recognized on the 4th layer line. Correspondingly, it is found from Fig. 8 that the intensity changes so slowly on the 4th layer plane that there is no sharp maxima producing the crystalline reflections. It is found thus that the stereocomplex of PLLA and PDLA should have as large shift disorder parameter as 0.1.

Figure 9 shows that lamellar crystals of the complex of PLLA and PDLA are basically triangular in morphology. Three sides of the lamellae correspond to any of 110, $\bar{2}10$ and $1\bar{2}0$ planes, respectively, on which PLLA and PDLA chains are alternatively deposited. As seen in Fig. 9, two spirals with the difference of 60° in rotation angle and sawtoothed growth on the growth front (maybe caused by twinning) occur very often. Figure 10 shows a matured crystal of the complex together with homopolymer lamellae of PLLA or PDLA with α-form. It has a characteristic round morphology although homopolymer lamellae have a definite shape. It is interesting that though the matured crystal has no definite morphology, it exhibits a sharp electron diffraction pattern with the hexagonal symmetry as the triangle lamellae. As a result of frequent

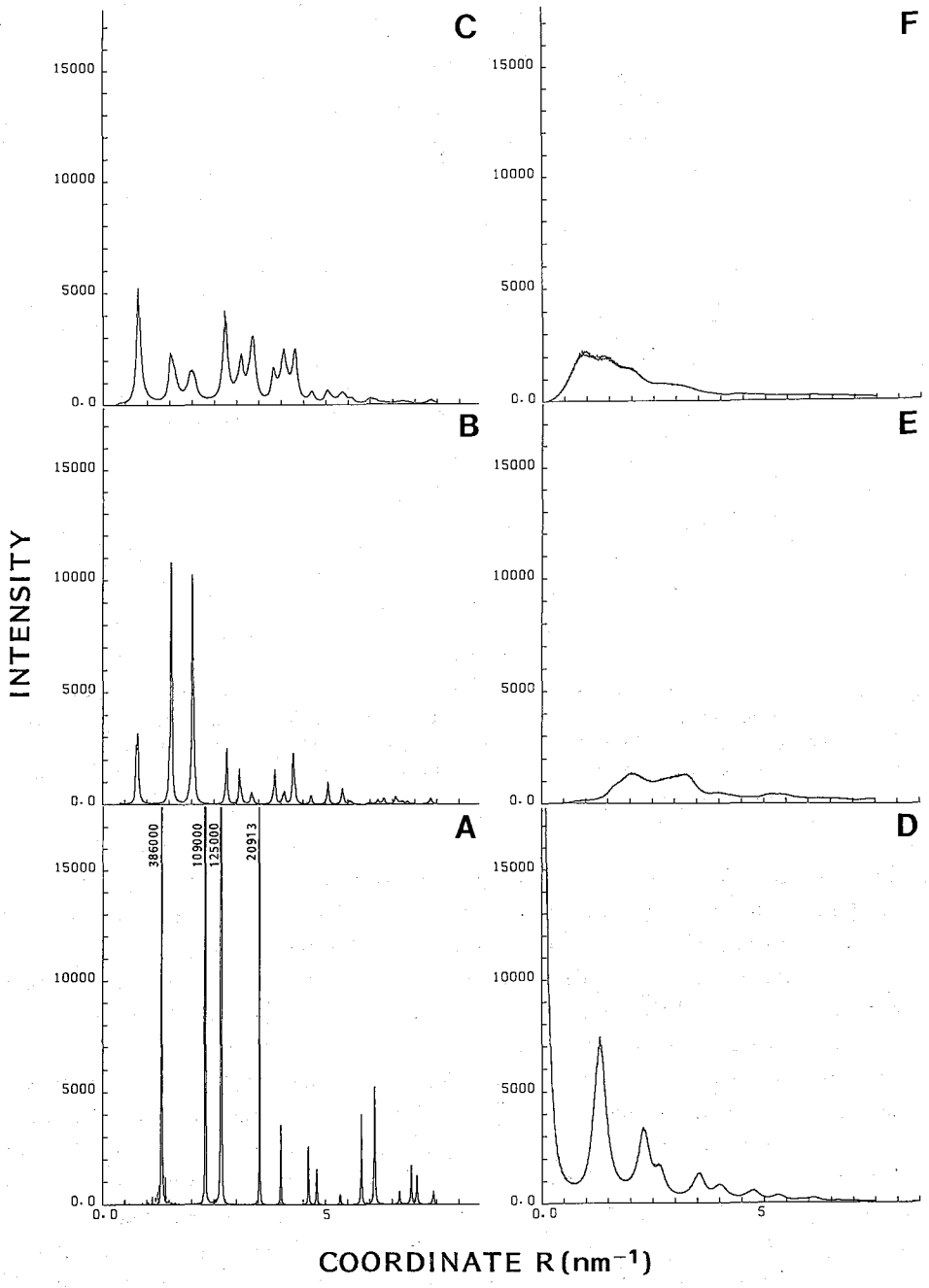

Figure 7. Patterns of A to F shows the calculated X-ray diffraction profiles on the zeroth to fifth layer line, respectively.

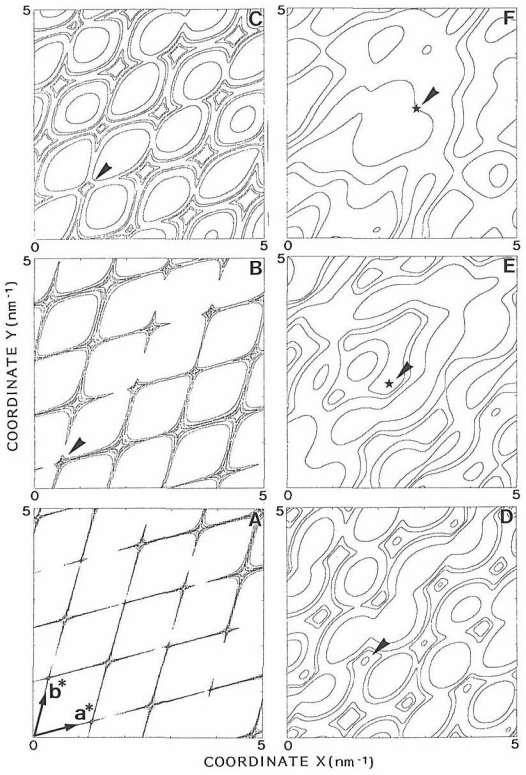

Figure 8. Simulated intensity maps developed on the layer planes. Maps of A to F correspend to the profiles of A to F in Fig. 7, respectively. Contour lines are drawn at the intensities of 100, 500, 1000, 5000 and 10000. The reciprocal axes a* and b* of the unit cell are shown by arrows in A. Positions shown by arrows in B to F indicate the 001, 002, 003, 004 and 005 reciprocal lattice points of the unit cell, respectively.

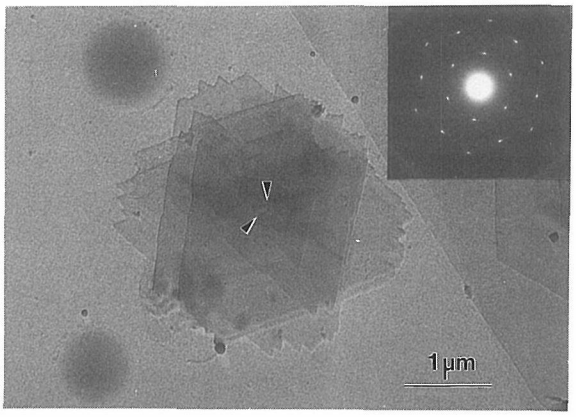

Figure 9. Electronmicrograph of the solution-grown lamella of the complex of PLLA and PDLA and the corresponding electron diffraction pattern. Arrows indicate the positions of the axes of the screw dislocations.

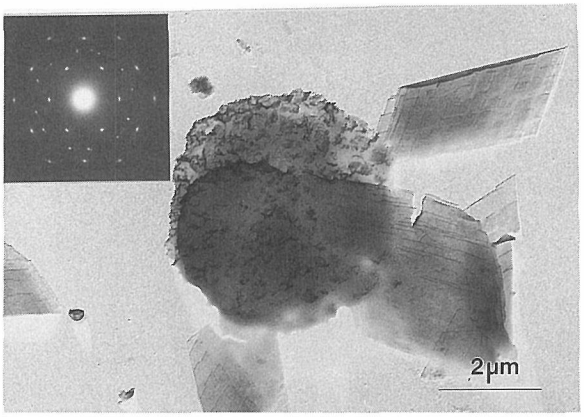

Figure 10. Electronmicrograph of the solution-grown, matured crystal of PLLA and PDLA complex and the corresponding electron diffraction pattern. Parallelogrammic lamellae are homopolymer crystals with α-form of PLLA or PDLA.

occurrence of such spiral growth and sawtoothed growth, the triangle lamellae may become round as they grow. Whenever daughter crystals grow on the mother crystals by these growth processes, their orientation always changes by 60° in rotation. The resulted electron diffraction pattern does not change from that of the triangular basic lamellae in appearance because their electron diffraction pattern is hexagonally symmetrical. The small crystallite size in drawn fibers (though not measured on the solution-grown crystals, the crystallite size may be small as well) may be due to these growth mechanisms; molecular chains are densely packed side-by-side but the coherent crystalline regions do not grow up largely and are limited laterally by change in growth direction due to frequent occurrece of these processes. As described above, polylactide chains in the stereocomplex are laterally packed with large fluctuation of shift in the direction parallel to their axis. The large fluctuations may induce the spiral growth of lamellar crystals, as molecular chains are displaced along their axis around the center of screw dislocation. Thus, the driving force of these growth modes is probably the large shift disorder among chains in the molecular directions.

REFERENCES

1) T. Okihara, M. Tsuji, A. Kawaguchi, K. Katayama, H. Tsuji, S. H. Hyon and Y. Ikada, to be published on J. Macromol. Sci.
2) K. Suehiro, Y. Chatani and H. Tadokoro, *Polymer J.*, **3**, 591 (1975).
3) R. Hosemann and S. N. Bagchi, "Direct analysis of diffraction by matter", North-Holland, Amsterdam, 1962.
4) B. K. Vainshtein, "Diffraction of X-rays by chain molecules", Elsevier, Amsterdam, 1966.
5) J. Petermann and R. M. Gohil, *J. Mater. Sci.*, **14**, 2260 (1979).
6) Y. Ikada, K. Jamshidi, H. Tsuji and S.-H. Hyon, *Macromolecules*, **10**, 996 (1987).
7) H. P. Klung and L. E. Alexander, "X-ray diffraction procedures", John Wiley & Sons, New York, 1974.
8) R. Hosemann and W. Wilke, *Makromol. Chem.* **118**, 230 (1968).
9) R. Hosemann, *Acta Cryst.*, **4**, 520 (1951).